Enhancement of Photoinduced Charge-Order Melting via Anisotropy Control by Double-Pulse Excitation in Perovskite Manganites: $Pr_{0.6}Ca_{0.4}MnO_3$

H. Yada,[1] Y. Ijiri,[1] H. Uemura,[1] Y. Tomioka,[2] and H. Okamoto[1]

[1]*Department of Advanced Materials Science, University of Tokyo, Kashiwa, Chiba 277-8561, Japan*
[2]*National Institute of Advanced Industrial Science and Technology (AIST), Tsukuba, Ibaraki 305-8561, Japan*

To control the efficiency of photoinduced charge-order melting in perovskite manganites, we performed femtosecond pump-probe spectroscopy using double-pulse excitation on $Pr_{0.6}Ca_{0.4}MnO_3$. The results revealed that the transfer of the spectral weight from the near-infrared to infrared region by the second pump pulse is considerably enhanced by the first pump pulse and that the suppression of crystal anisotropy, that is, the decrease of long-range lattice deformations due to the charge order by the first pump pulse is a key factor to enhance the charge-order melting. This double-pulse excitation method can be applied to various photoinduced transitions in complex materials with electronic and structural instabilities.

Perovskite-type manganites exhibit various electronic phases such as a Mott insulator phase, antiferromagnetic charge-order insulator (COI) phase, and ferromagnetic metal (FM) phase, which originate from the strong interplay between electron, spin, and orbital degrees of freedom [1,2]. In nearly half-doped manganites, in particular, COI and FM phases sometimes compete against each other, so that dramatic COI-to-FM transitions are driven by applications of external perturbations such as magnetic fields, electric fields, and pressure [3]. In addition to such perturbations, a photoirradiation has been utilized to control rapidly the electronic states in the COI phase [4–17] and other phases [18–26]. In a typical half-doped manganite, $Nd_{0.5}Ca_{0.5}MnO_3$, pump-probe (PP) spectroscopy revealed that an irradiation of a femtosecond laser pulse in the COI phase induces the partial transfer of the spectral weight from the gap transition to the lower-energy region and the decrease of the anisotropy in the optical conductivity spectra due to the CE-type CO [6,8]. These results showed that the CO was weakened but not completely melted by light. In nearly half-doped manganites such as $Nd_{1-x}Sr_xMnO_3$ and $Pr_{1-x}Ca_xMnO_3$ $(0.4 < x \leq 0.5)$, the situation was the same as that in $Nd_{0.5}Ca_{0.5}MnO_3$; the CO is robust and the photoinduced CO melting is difficult to be achieved.

To enhance the efficiency of the photoinduced CO melting, selected was another nearly half-doped manganite, $Gd_{0.55}Sr_{0.45}MnO_3$, in which the long-range CO is disturbed by the larger variance (i.e., disorder) of the ionic radii of A-site cations [27], and instead short-range CO with no crystal anisotropy is formed. In this compound, the short-range CO was almost melted by the irradiation of a femtosecond laser pulse and the FM state subsequently appeared [5]. This result suggests that the destruction of the crystal anisotropy would be a key factor to enhance the efficiency of a photoinduced CO melting [15]. The isotropic phase in

$Gd_{0.55}Sr_{0.45}MnO_3$ is exceptional and the other CO manganites have strong crystal anisotropy due to the CO in common. Therefore, a new method is desirable to enhance the efficiency of the photoinduced CO melting in the anisotropic CO manganites.

From these backgrounds, in the present study, we apply a double-pulse excitation method to a prototypical nearly half-doped manganite, $Pr_{0.6}Ca_{0.4}MnO_3$. In this method, the first pump pulse with various fluences is introduced to prepare the CO states with different crystal anisotropy, which is subsequently excited with the second pump pulse. Then the CO melting efficiency is detected by a probe pulse.

In a half-doped manganite, $Pr_{0.5}Ca_{0.5}MnO_3$, a CE-type CO is stabilized in an orthorhombic structure [Fig. 1(a)], in which half of the c-axis lattice constant, $c/2$ (0.3753 nm), is shortened compared with $(a + b)/\sqrt{2}$ (0.3853 nm) at 80 K [28] with the elongations of d orbitals in the ab plane. $Pr_{0.6}Ca_{0.4}MnO_3$ shows a transition from paramagnetic insulator to COI at $T_{CO} \sim 235$ K [29]. Figure 1(b) shows charge, orbital, and spin structures of this compound [30], which can be understood by considering excess electrons of 0.1 per Mn added to $Pr_{0.5}Ca_{0.5}MnO_3$. The orbital of an excess electron is elongated along the c axis as shown by dotted lines, resulting in the reduction of the crystal anisotropy. In fact, the orthorhombic distortion in the COI phase of $Pr_{0.6}Ca_{0.4}MnO_3$ (0.43%) is smaller than that of $Pr_{0.5}Ca_{0.5}MnO_3$ (1.1%) [30].

Single crystals of $Pr_{0.6}Ca_{0.4}MnO_3$ were grown by the floating-zone method [29,31]. (100) cut crystals were used for optical measurements. Crystal surfaces were polished and annealed at 1000°C in an oxygen atmosphere to relax strains for optical reflectivity measurements [5,8,14]. In PP reflection spectroscopy, a Ti:sapphire regenerative amplifier (RA) with photon energy of 1.58 eV, a pulse width of 120 fs, and a repetition rate of 1 kHz was used as a light source. Output from the RA was divided to two paths.
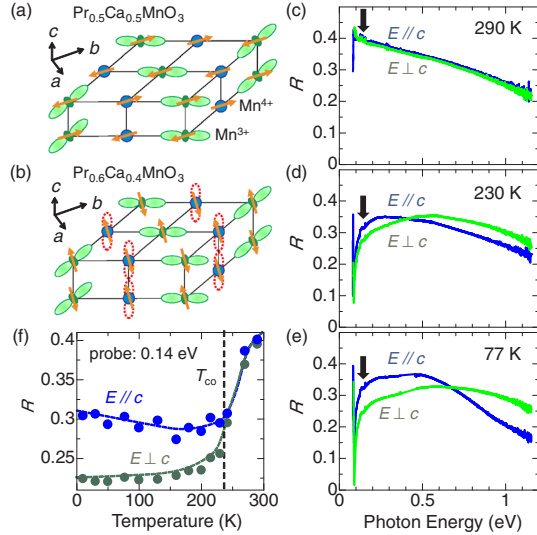
FIG. 1. Charge, orbital-order, and spin structures of $Pr_xCa_{1-x}MnO_3$ in (a) $x = 0.5$ and (b) $x = 0.4$ [19]. (c)–(e) Polarized reflectivity (R) spectra of $Pr_{0.6}Ca_{0.4}MnO_3$ at typical temperatures. (f) Temperature dependences of R values at 0.14 eV.

One was used as a pump pulse and the other was used as an excitation source of an optical parametric amplifier (OPA) for generating a probe pulse (0.1–0.85 eV). Delay time t_d of the probe pulse relative to the pump pulse is controlled by changing the path length of the pump pulse. For double-pump experiments, a pump pulse is further divided to two paths and united again by means of a Michelson-type optical system.

First, we briefly discuss the temperature dependence of the crystal anisotropy and electronic structure in $Pr_{0.6}Ca_{0.4}MnO_3$. Figures 1(c)–1(e) show polarized reflectivity (R) spectra with electric fields of light E parallel (//) and perpendicular ($\perp$) to the c axis. At 77 and 230 K the magnitude of R below 0.4 eV along c ($E//c$) is larger than that along the ab plane ($E \perp c$). This is attributable to excess electrons in the d orbitals along c as mentioned above. On the other hand, at 290 K, R spectra do not show anisotropy, reflecting the disappearance of CO. In this study, we use as a measure of the anisotropy the polarization dependence of R at 0.14 eV [arrows in Figs. 1(c)–1(e)], the temperature dependence of which was shown in Fig. 1(f).

Next we show the results of PP measurements with a single pump pulse. The pump photon energy (1.58 eV) is located in the higher-energy side of the intermanganese transition extending from 0.2 to 1.2 eV [32]. The electric field E_{pump} of the pump pulse was $\perp c$, in common. Figure 2(b) shows photoinduced change ($\Delta R/R$) of the R spectrum ($E_{probe} \perp c$) at 77 K [Fig. 2(a)] with the excitation photon densities (x_{ph}) of 0.094 and 0.049 photon/Mn site (ph/Mn) [33] just after the photoirradiation ($t_d = 0.2$ ps) and at $t_d = 4$ ps. $\Delta R/R$ at $t_d = 0.2$ ps (solid circles and triangles) is positive below 0.6 eV, showing that the system becomes conductive by the
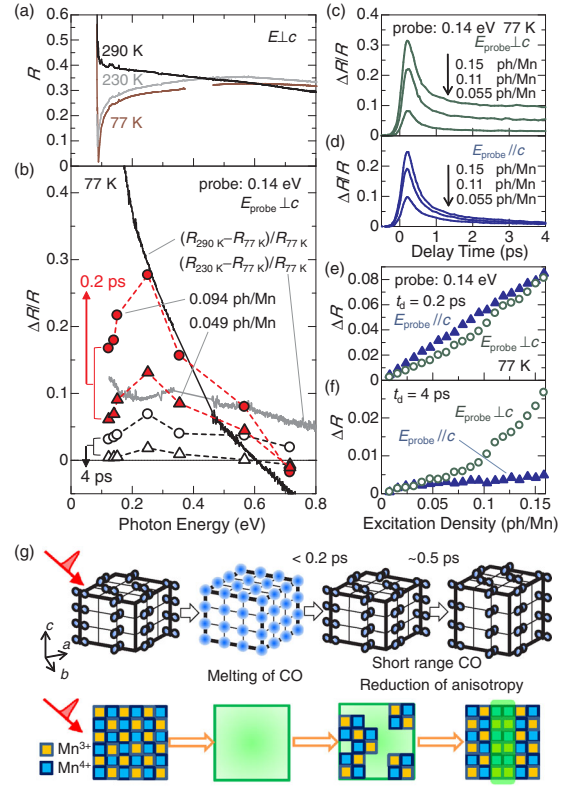
FIG. 2. (a) Polarized reflectivity spectra ($E \perp c$) [taken from Figs. 1(c)–1(e)]. (b) Transient $\Delta R/R$ spectra. Differential reflectivities $(R_{290 K} - R_{77 K})/R_{77 K}$ and $(R_{230 K} - R_{77 K})/R_{77 K}$ (solid lines). (c), (d) Time evolutions of $\Delta R/R$. (e),(f) x_{ph} dependence of polarized $\Delta R/R$ at 0.14 eV. (g) Schematics dynamics of CO, orbital-order, and lattice anisotropy after the photoexcitation.

photoirradiation. In Fig. 2(b), we also showed differential reflectivity spectra ($E \perp c$), $(R_{290 K} - R_{77 K})/R_{77 K}$ between 290 K ($> T_{CO}$) and 77 K, and $(R_{230 K} - R_{77 K})/R_{77 K}$ between 230 K ($\leq T_{CO}$) and 77 K. Magnitudes of $\Delta R/R$ at $t_d = 0.2$ ps for 0.094 ph/Mn (0.049 ph/Mn) are comparable to those of $(R_{290 K} - R_{77 K})/R_{77 K}$ [$(R_{230 K} - R_{77 K})/R_{77 K}$], while the spectral shape of the former is different from the latter. $\Delta R/R$ shows a peak at ~0.25 eV. This indicates that the original CO is not completely melted and photoinduced phases are different from steady-state phases.

Figures 2(c) and 2(d) show time evolutions of $\Delta R/R$ at 0.14 eV measured at 77 K with $E_{probe} \perp c$ and $E_{probe}//c$, respectively. In all results, an ultrafast increase of R just after the photoirradiation, its rapid decrease within ~0.5 ps, and a slow-decay component are observed in common. The ultrafast increase of R is due to the partial melting of CO by photocarrier generations as mentioned above. This component is almost proportional to x_{ph} [Fig. 2(e)]. The decrease of $\Delta R/R$ up to 0.5 ps is attributable to photocarrier recombination and the resultant recovery of CO. Such subpicosecond responses were also observed in other CO manganites [6,15]. To interpret the slow-decay

components, heating effects should be taken into account. The temperature dependence of R [Fig. 1(f)] shows that the increase of temperature should induce negative $\Delta R/R$ signals for $E_{\text{probe}}//c$. However, $\Delta R/R$ was positive at $t_d = 4$ ps for all the x_{ph} values [Fig. 2(f)] for $E_{\text{probe}}//c$ as well as for $E_{\text{probe}}\perp c$. Therefore, $\Delta R/R$ signals for $t_d > 0.5$ ps cannot be explained by a simple heating of the system, but might be attributed to a new photoinduced state or a kind of hidden state [16], which is more conductive than the original state.

At high excitation densities above 0.05 ph/Mn, $\Delta R/R$ at $t_d = 4$ ps for $E_{\text{probe}}\perp c$ is 1.3 to 5.4 times as large as that for $E_{\text{probe}}//c$ [Fig. 2(f)], which is in contrast to the small polarization dependence in $\Delta R/R$ at $t_d = 0.2$ ps. This means that for $t_d > 0.5$ ps the original difference of R between two polarizations is decreased and the photo-induced state is more isotropic as well as more conductive. In addition, this state is long-lived up to ~ 300 ps (not shown). A possible assignment of such a long-lived, more conductive, and more isotropic state photoinduced is a short-range CO state schematically shown in Fig. 2(g). In this state, we consider that some of the photocarriers are stabilized as polarons, being long-lived due to the low mobility. These polarons would exist probably between neighboring CO domains, making the system more con-ductive than the original long-range CO state. The more isotropic nature of this photoinduced state is attributable to the fact that some CO states would be formed along the c axis during the initial rapid recovery process of the CO. This state hardly returns to the original CO state along the ab plane so that it is long-lived.

In order to characterize the photoinduced complex changes of the CO, we introduce two parameters, ΔI_c and ΔI_a, expressed as follows:

$$\Delta I_c = -\frac{(\Delta R_{//} + \Delta R_{\perp})_{77 \text{ K}}}{(R_{//} + R_{\perp})_{290 \text{ K}} - (R_{//} + R_{\perp})_{77 \text{ K}}},$$

$$\Delta I_a = \frac{(\Delta R_{//} - \Delta R_{\perp})_{77 \text{ K}}}{(R_{//} - R_{\perp})_{77 \text{ K}}}. \quad (1)$$

Here, $R_{//}$ and $R_{\perp}$ represent R values at 0.14 eV for $E_{\text{probe}}//c$ and $E_{\text{probe}}\perp c$, respectively. ΔI_c and ΔI_a re-present the ratios of the decreases in the microscopic (or local) amplitude of the CO and in the crystal anisotropy originating from the long-range CO, respectively. The derivation of Eq. (1) is detailed in the Supplemental Material [34]. x_{ph} dependences of these two parameters at $t_d = 4$ ps were shown in Fig. 3(a). ΔI_c and ΔI_a were evaluated to be -5.9% and -9.9%, respectively, at $x_{\text{ph}} = 0.1$ ph/Mn. Thus, the crystal anisotropy as well as the local CO amplitude can be controlled for $t_d > 0.5$ ps by changing x_{ph}.

Next, we discuss the results of double-pump experi-ments. First, the temporal spacing of two pump pulses (t_{12})
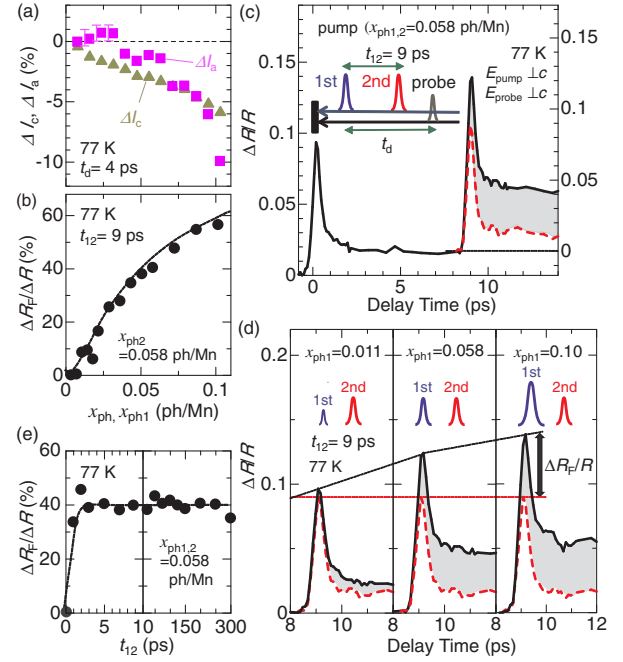
FIG. 3. (a) x_{ph} dependence of decreases in CO amplitudes (ΔI_c) and anisotropy (ΔI_a) at $t_d = 4$ ps. (b) x_{ph1} dependence of $\Delta R_F/\Delta R$ just after the 2nd pulse. (c) Time evolutions of $\Delta R/R$ with (solid line) and without 1st pulse (broken line). The inset is a schematic of a double-pulse-pump and probe measurements. (d) Time evolutions of $\Delta R/R$ for several x_{ph1} values, whose offsets are subtracted. Broken red lines show $\Delta R/R$ without 1st pump. (e) t_{12} dependence of $\Delta R_F/\Delta R$.

was fixed to be 9 ps. Figure 3(c) shows the time evolutions of $\Delta R/R$ for $E_{\text{probe}}\perp c$. Excitation photon densities of the 1st pump pulse (x_{ph1}) and 2nd pump pulse (x_{ph2}) were both set at 0.058 ph/Mn. Just after the 2nd pump, $\Delta R/R$ was increased additionally on the tail of the $\Delta R/R$ signal due to the 1st pump. The broken line in the same figure shows the $\Delta R/R$ signal when the sample was irradiated with only the 2nd pump. That is plotted as the zero line accords with the long-lived tail of $\Delta R/R$ by the 1st pump (the dotted line). The net $\Delta R/R$ signal by the 2nd pump is consid-erably larger than that only by the 2nd pump (the broken line) in Fig. 3(c). The increase in the second-pump-induced reflectivity change ($\Delta R_F/\Delta R$) under the presence of the 1st pump (shaded area) compared with the reflectivity change ($\Delta R/R$) by the 2nd pump alone is hereafter denoted as $\Delta R_F/\Delta R$ and called the enhancement factor.

To further investigate the effect of the 1st pump on $\Delta R_F/\Delta R$ by the 2nd pump, x_{ph1} was changed, while x_{ph2} was constant (0.058 ph/Mn). Figure 3(d) shows net $\Delta R/R$ signals by the 2nd pump (solid lines) together with $\Delta R/R$ signals by the 2nd pump alone (broken lines). When the 1st pump is weak ($x_{\text{ph1}} = 0.011$ ph/Mn), the enhancement $\Delta R_F/\Delta R$ (the gray shaded area) is small. But, it was considerably enlarged with increase of x_{ph1}.

In Fig. 3(b), we plotted the enhancement factor $\Delta R_F/\Delta R$ just after the 2nd pump [the arrow in Fig. 3(d)] as a function

of x_{ph1}, which is the ratio of the enhancement of net reflectivity changes just after the 2nd pump by the presence of the 1st pump. With increase of x_{ph1}, $\Delta R_F/\Delta R$ monotonically increases, reaching $\sim 60\%$ at $x_{ph1} = 0.1$ ph/Mn. It corresponds well to the decreases of the CO amplitude (ΔI_c) and the crystal anisotropy (ΔI_a) with increase of x_{ph} [Fig. 3(a)]. To further confirm the enhancement, we evaluated $\Delta R_F/\Delta R$ for $x_{ph1} = x_{ph2} = 0.058$ ph/Mn as a function of the interval between the 1st and 2nd pump pulses (t_{12}), which was shown in Fig. 3(e). $\Delta R_F/\Delta R$ is almost constant for 0.5 ps $< t_{12} <$ 300 ps, while $\Delta R_F/\Delta R$ at $t_{12} = 0$ ps is zero [35]. This result demonstrates that the effect of the 1st pump, which accelerates the photoinduced CO melting by the 2nd pump, occurs after a finite time ($>$ the time resolution of 200 fs) and persists at least up to 300 ps.

The excitation-photon-density dependence of ΔI_c and ΔI_a in Fig. 3(a) shows that the local CO amplitude is decreased and the crystal anisotropy is suppressed with an increase of x_{ph1}. As shown in Fig. 2(e), however, the CO melting just after the photoirradiation shows a linear dependence on the excitation density. Therefore, it is reasonable to consider that the decrease of the local CO amplitude by the 1st pump is not the main cause for the nonlinear enhancement of the CO melting by the 2nd pump. This result indicates that the decrease of the crystal anisotropy is more important for the enhancement of the CO melting by the 2nd pump than the decrease of the local CO amplitude.

To obtain information about the nature of photoinduced states after the 2nd pump, we measured the probe-energy dependence of $\Delta R_F/\Delta R$ with $x_{ph1} = 0.094$ ph/Mn and $x_{ph2} = 0.049$ ph/Mn and constructed a spectrum of the enhancement factor, $\Delta R_F/\Delta R$. The result is shown in Fig. 4(b) together with the $\Delta R/R$ spectrum at $t_d = 0.2$ps by a single pump in Fig. 4(a). The $\Delta R_F/\Delta R$ spectrum clearly shows that the spectral weight transfer to the low-energy region is enhanced due to the presence of the 1st pump. These results suggest that short range CO states with weakened anisotropy prepared by the 1st pump are more sensitive to the photoexcitation and that the photoinduced CO melting by the 2nd pump is accelerated and the final state becomes more conductive.

It is valuable to compare the final state generated by double pump pulses (x_{ph1} and x_{ph2}) with the state generated by a single pump pulse with a fluence larger than ($x_{ph1} + x_{ph2}$). For this purpose, we plotted in Fig. 4(b) ($\Delta R_H - \Delta R_L$)/ΔR_L, in which ΔR_H and ΔR_L are the reflectivity changes by a single pump with $x_{ph} = 0.094$ and 0.049 ph/Mn, respectively. The ($\Delta R_H - \Delta R_L$)/ΔR_L spectrum does not show a strong tendency of the spectral-weight transfer to the lower energy, but has positive values over the wide energy region, differently from the $\Delta R_F/\Delta R$ spectrum. It can be understood by the fact that by a single pump, most of photocarriers decay before the decrease of the crystal anisotropy, the characteristic time of which will
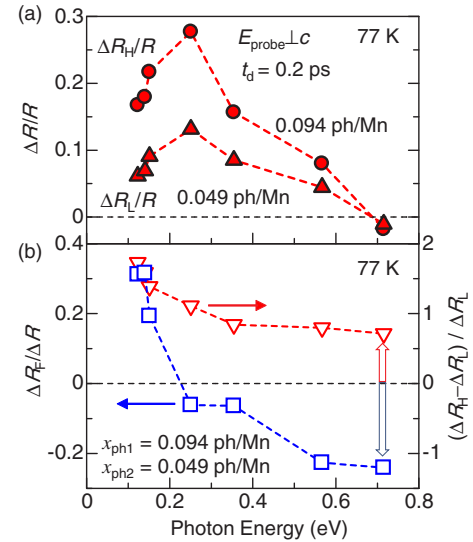
FIG. 4. (a) $\Delta R/R$ spectra. ΔR_H and ΔR_L are the reflectivity changes by a single pump with $x_{ph} = 0.094$ and 0.049 ph/Mn [Fig. 2(b)], respectively. (b) $\Delta R_F/\Delta R$ and ($\Delta R_H - \Delta R_L$)/ΔR_L spectra.

be longer than the decay time of photocarriers (a few hundreds of femtoseconds) [5,6]. It is reasonable since anisotropy changes should be accompanied by structural deformations. Thus, the double-pulse excitation is an effective method to drive the photoinduced transition, including both fast electronic responses (the decrease of the local CO amplitudes) and slower structural changes (the decrease of the anisotropy).

In summary, we performed double-pulse pump experiments in $Pr_{0.6}Ca_{0.4}MnO_3$. By a single-pulse pump, the long-range CO is converted to the short-range CO with the smaller CO amplitude, and the crystal anisotropy is weakened. By a double-pulse pump, photoinduced melting of CO is enhanced by $\sim 60\%$ as compared to the single-pulse pump. The scrutiny of the results suggests that the decrease of the crystal anisotropy is a key factor for enhancing the efficiency of the photoinduced CO melting.

[1] E. Dagotto, Science **309**, 257 (2005).
[2] Y. Tokura, Rep. Prog. Phys. **69**, 797 (2006).
[3] *Colossal Magnetoresistive Oxides*, edited by Y. Tokura (Gordon and Breach, London, 1999).
[4] M. Fiebig, K. Miyano, Y. Tomioka, and Y. Tokura, Appl. Phys. B **71**, 211 (2000).
[5] M. Matsubara, Y. Okimoto, T. Ogasawara, Y. Tomioka, H. Okamoto, and Y. Tokura, Phys. Rev. Lett. **99**, 207401 (2007).
[6] H. Matsuzaki, H. Uemura, M. Matsubara, T. Kimura, Y. Tokura, and H. Okamoto, Phys. Rev. B **79**, 235131 (2009).

[7] K. Miyano, T. Tanaka, Y. Tomioka, and Y. Tokura, Phys. Rev. Lett. **78**, 4257 (1997).

[8] T. Ogasawara, K. Tobe, T. Kimura, H. Okamoto, and Y. Tokura, J. Phys. Soc. Jpn. **71**, 2380 (2002).

[9] N. Takubo, Y. Ogimoto, M. Nakamura, H. Tamaru, M. Izumi, and K. Miyano, Phys. Rev. Lett. **95**, 017404 (2005).

[10] K. Miyasaka, M. Nakamura, Y. Ogimoto, H. Tamaru, and K. Miyano, Phys. Rev. B **74**, 012401 (2006).

[11] R. P. Prasankumar, S. Zvyagin, K. V. Kamenev, G. Balakrishnan, D. M. Paul, A. J. Taylor, and R. D. Averitt, Phys. Rev. B **76**, 020402(R) (2007).

[12] Y. Okimoto, H. Matsuzaki, Y. Tomioka, I. Kezsmarki, T. Ogasawara, M. Matsubara, H. Okamoto, and Y. Tokura, J. Phys. Soc. Jpn. **76**, 043702 (2007).

[13] M. Rini, R. Tobey, N. Dean, J. Itatani, Y. Tomioka, Y. Tokura, R. W. Schoenlein, and A. Cavalleri, Nature (London) **449**, 72 (2007).

[14] M. Matsubara, Y. Okimoto, T. Ogasawara, S. Iwai, Y. Tomioka, H. Okamoto, and Y. Tokura, Phys. Rev. B **77**, 094410 (2008).

[15] M. Matsubara, T. Ogasawara, Y. Tomimoto, K. Tobe, H. Okamoto, and Y. Tokura, J. Phys. Soc. Jpn. **78**, 023707 (2009).

[16] H. Ichikawa, S. Nozawa, T. Sato, A. Tomita, K. Ichiyanagi, M. Chollet, L. Guerin, N. Dean, A. Cavalleri, S. Adachi, T. Arima, H. Sawa, Y. Ogimoto, M. Nakamura, R. Tamaki, K. Miyano, and S. Koshihara, Nat. Mater. **10**, 101 (2011).

[17] T. Mertelj, D. Mihailovic, Z. Jagličič, A. A. Bosak, O. Y. Gorbenko, and A. R. Kaul, Phys. Rev. B **68**, 125112 (2003).

[18] Y. G. Zhao, J. J. Li, R. Shreekala, H. D. Drew, C. L. Chen, W. L. Cao, C. H. Lee, M. Rajeswari, S. B. Ogale, R. Ramesh, G. Baskaran, and T. Venkatesan, Phys. Rev. Lett. **81**, 1310 (1998).

[19] A. I. Lobad, R. D. Averitt, C. Kwon, and A. J. Taylor, Appl. Phys. Lett. **77**, 4025 (2000).

[20] A. I. Lobad, R. D. Averitt, and A. J. Taylor, Phys. Rev. B **63**, 060410 (2001).

[21] R. D. Averitt, A. L. Lobad, C. Kwon, S. A. Trugman, V. K. Thorsmølle, and A. J. Taylor, Phys. Rev. Lett. **87**, 017401 (2001).

[22] Y. H. Ren, M. Ebrahim, H. B. Zhao, G. Lüpke, Z. A. Xu, V. Adyam, and Q. Li, Phys. Rev. B **78**, 014408 (2008).

[23] K. H. Wu, T. Y. Hsu, H. C. Shih, Y. J. Chen, C. W. Luo, T. M. Ueh, J.-Y. Lin, J. Y. Juang, and T. Kobayashi, J. Appl. Phys. **105**, 043901 (2009).

[24] T. Ogasawara, M. Matsubara, Y. Tomioka, M. Kuwata-Gonokami, H. Okamoto, and Y. Tokura, Phys. Rev. B **68**, 180407(R) (2003).

[25] S. A. McGill, R. I. Miller, O. N. Torrens, A. Mamchik, I. Wei Chen, and J. M. Kikkawa, Phys. Rev. B **71**, 075117 (2005).

[26] T. Mertelj, R. Yusupov, A. Gradišek, M. Filippi, W. Prellier, and D. Mihailovic, Europhys. Lett. **86**, 57003 (2009).

[27] Y. Tomioka and Y. Tokura, Phys. Rev. B **70**, 014432 (2004).

[28] F. Damay, C. Martin, A. Maignan, M. Herview, B. Raveau, F. Bourée, and G. André, Appl. Phys. Lett. **73**, 3772 (1998).

[29] Y. Tomioka, A. Asamitsu, H. Kuwahara, Y. Moritomo, and Y. Tokura, Phys. Rev. B **53**, R1689 (1996).

[30] Z. Jirák, S. Krupička, Z. Šimša, M. Dlouhá, and S. Vratislav, J. Magn. Magn. Mater. **53**, 153 (1985).

[31] Y. Tomioka, A. Asamitsu, Y. Moritomo, and Y. Tokura, J. Phys. Soc. Jpn. **64**, 3626 (1995).

[32] Y. Okimoto, Y. Tomioka, Y. Onose, Y. Otsuka, and Y. Tokura, Phys. Rev. B **59**, 7401 (1999).

[33] The excitation photon density x_{ph} was defined by the photon density per unit volume within the absorption depth and evaluated by $x_{ph} = (1 - 1/e)(1 - R_p)I_p/l_p$, where I_p, l_p, R_p, and e are the excitation photon density per unit area, the absorption depth, the reflection loss of the pump light, and Napier's constant, respectively.

[34] See Supplemental Material at http://link.aps.org/supplemental/10.1103/PhysRevLett.116.076402, which includes the definitions and physical meanings of the parameters, ΔI_c and ΔI_a.

[35] $\Delta R_F/R$ at $t_{12} = 0$ ps is assumed to be 0, since x_{ph} dependence of $\Delta R/R$ is almost linear [Fig. 2(e)].